

# Contributing Factors to the Recent High Level of Accumulated Cyclone Energy (ACE) and Power Dissipation Index (PDI) in the North Atlantic\*

HIROYUKI MURAKAMI

*International Pacific Research Center, University of Hawai'i at Mānoa, Honolulu, Hawaii, and Meteorological Research Institute, Tsukuba, Ibaraki, Japan*

TIM LI

*International Pacific Research Center, and Department of Meteorology, University of Hawai'i at Mānoa, Honolulu, Hawaii*

PANG-CHI HSU

*Key Laboratory of Meteorological Disaster, and College of Atmospheric Science, Nanjing University of Information Science and Technology, Nanjing, China, and International Pacific Research Center, University of Hawai'i at Mānoa, Honolulu, Hawaii*

(Manuscript received 8 July 2013, in final form 10 December 2013)

## ABSTRACT

In recent decades, tropical cyclone (TC) activity in the North Atlantic has shown a marked positive anomaly in genesis number, mean lifespan, number of intense hurricanes, and mean maximum intensity. The accumulated cyclone energy (ACE), which is defined as the sum of the square of the maximum surface wind velocity throughout the lifetime of a TC, is one of the measures that can be used to synthesize these factors. Similar to the ACE, the power dissipation index (PDI), which is defined as the integrated third power of maximum surface wind velocity, has also been used to describe TC activity. The basin-total ACE and PDI for the North Atlantic have also followed a large positive anomaly during the period 1995–2012; however, the relative importance of factors such as TC genesis number, TC track property (e.g., duration and lifespan), and TC intensity remains unclear in terms of their contribution to the positive anomalies in ACE and PDI. This study uses a new empirical statistical approach to analyze the TC data and finds that the increase in the TC genesis number is primarily responsible for the positive anomalies in ACE and PDI. Other factors, such as TC track property and TC intensity, appear to be minor influences.

## 1. Introduction

Figure 1 shows observed trends from the National Hurricane Center Best Track Database (HURDAT; Landsea et al. 2004; 1966–2012) for basin-total accumulated cyclone energy (ACE; Bell et al. 2000), power dissipation index (PDI; Emanuel 2005, 2007), tropical

cyclone (TC) genesis number, mean TC lifespan, TC number for major hurricanes (i.e., category 3 or above), and mean maximum TC intensity. This analysis reveals marked positive trends over the past 40 years in the North Atlantic, especially after 1995 (Elsner et al. 2004; Emanuel 2005; Webster et al. 2005; Klotzbach 2006). These positive trends are statistically significant at the 99% level using both the Student's  $t$  test for the slopes and the modified Mann–Kendall test (Hamed and Rao 1998), for which autocorrelations in the input data (i.e., 7-yr running mean data) are considered.<sup>1</sup> Elsner et al. (2004) also pointed out an abrupt shift in number of

---

\* School of Ocean and Earth Science and Technology Publication Number 9065 and International Pacific Research Center Publication Number 1039.

---

Corresponding author address: Hiroyuki Murakami, International Pacific Research Center (IPRC), 1680 East-West Road, University of Hawai'i at Mānoa, Honolulu, HI, 96822.  
E-mail: hir.murakami@gmail.com

---

<sup>1</sup> If the significance test is applied to annual mean data, linear trends in mean TC lifespan and TC intensity are not statistically significant.

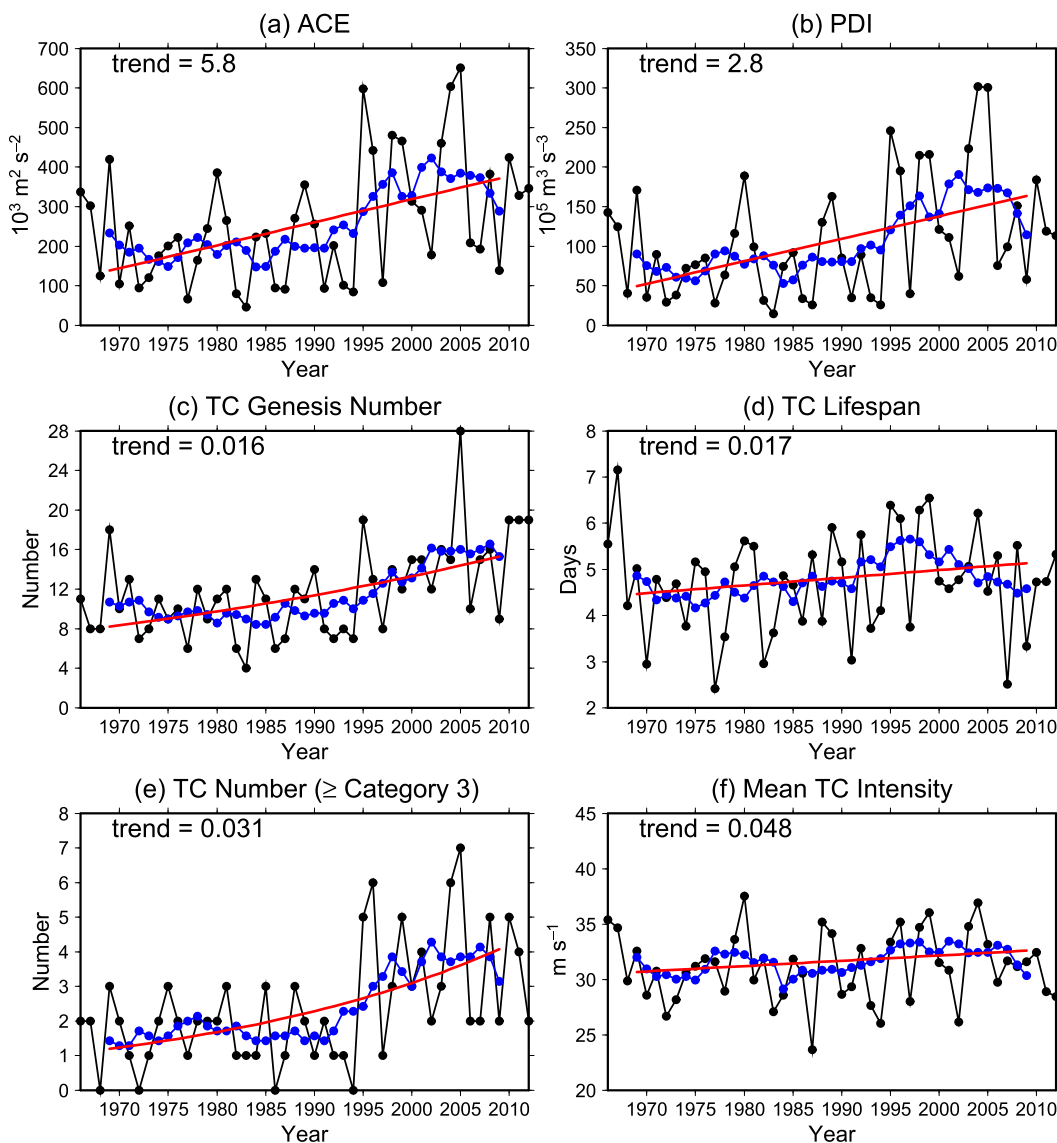


FIG. 1. Interannual variations in various metrics for TC activity during 1966–2012 from HURDAT best-track data. (a) Accumulated cyclone energy (ACE;  $10^3 \text{ m}^2 \text{ s}^{-2}$ ). (b) Power dissipation index (PDI;  $10^5 \text{ m}^3 \text{ s}^{-3}$ ). (c) TC genesis number (number). (d) Mean TC lifespan (days). (e) TC number of category 3 or above (number). (f) Mean maximum TC intensity ( $\text{m s}^{-1}$ ). Black lines indicate annual mean, blue lines denote 7-yr running mean, and red lines show linear trend from the 7-yr running mean by the least squares regression for (a),(b),(d), and (f) and by the Poisson regression for (c) and (e). The number in the top left corner of each panel shows the slope of the linear trend.

major hurricanes in 1995. These positive trends, or abrupt shift, have aroused public interest regarding their relationship to global warming (Emanuel 2005; Webster et al. 2005); however, the nature and extent of this relationship remains in dispute due to the short period for which reliable satellite observations are available (Landsea et al. 2006), and also because of the inherent natural variability of the system (Knutson et al. 2010).

ACE and the PDI are indices that incorporate the TC genesis frequency, TC lifespan, and TC intensity. Therefore, their total values in a particular basin can be

used as a measure of overall TC activity. The ACE is used to express the activity and destructive potential of individual TCs and can therefore be used as a measure of potential storm-related damage. The total annual ACE for the North Atlantic is reported every year in the “State of the Climate” report issued by the American Meteorological Society (Bell et al. 2013). The temporal variations in PDI for the North Atlantic have also been examined. Recent studies have focused on the statistical linkage of PDI variations to sea surface warming in the Atlantic in both observations (Emanuel 2007; Villarini

and Vecchi 2012) and future projections (Vecchi and Soden 2007). However, an open question remains: which of the several likely influencing factors contributes most to the recent high level of ACE and PDI? Figure 1 shows that the TC genesis number and number of intense TC (category 3 or above) follow marked positive trends, whereas mean TC intensity and lifespan show less pronounced positive trends. However, because ACE (PDI) is the cumulative total of the square (cube) of maximum surface wind speed, a small increase in mean TC intensity could have caused a substantial increase in ACE (PDI). To identify the factors responsible for the recent high level of ACE and PDI in the North Atlantic, we developed a new diagnosis method that incorporates and extends previous approaches (Yokoi and Takayabu 2013; Murakami et al. 2013, 2014). The remainder of this paper is organized as follows. Section 2 provides input data and analysis methodology and section 3 presents the results. Finally, a summary and discussion are given in section 4.

## 2. Methods

### a. Data

For the input data, we used the 6-hourly HURDAT best-track data from the period 1966–2012, because basinwide monitoring via satellite began in 1966 (Landsea 2007), and only considered storms while they were in either their tropical or subtropical stages as designated in the HURDAT dataset. Landsea (1993) provided a correction for the wind speed for the intense TCs before 1970 using the following equation:

$$V_{\max} = 7(1013 - P_c)^{0.5}, \quad (1)$$

where  $V_{\max}$  is the corrected maximum sustained wind speed ( $\text{m s}^{-1}$ ) and  $P_c$  is the minimum sea level pressure (hPa). Following Landsea (1993), we applied this correction to wind speed velocity in excess of 45 kt ( $1 \text{ kt} = 0.51 \text{ m s}^{-1}$ ) for the data before 1970; however, the effect of this correction is minimal at best and does not affect any conclusions reached in this study.

### b. Empirical statistical analysis

The new empirical statistical analysis of ACE and PDI can reveal the quantitative contribution of four factors (TC genesis, TC track, TC intensity, and the nonlinearity of the previous three factors) to the positive anomaly in ACE and PDI. We conducted two types of analyses (total and origin) to investigate domainwide and location-specific effects. The empirical statistical analysis of ACE is described below. The description for

the analysis of PDI is omitted because it can be conducted by replacing the square of wind speed in the ACE analysis with the cube of wind speed.

In a similar fashion to Yokoi and Takayabu (2013), we considered the ACE for each grid cell ( $10^\circ \times 10^\circ$ ) within the North Atlantic domain ( $0^\circ\text{--}50^\circ\text{N}$ ,  $0^\circ\text{--}100^\circ\text{W}$ ), before discussing total ACE in specific regions and the domain as a whole. In general, ACE is defined as the accumulated cyclone energy throughout the lifetime of a TC (i.e., Lagrangian approach); however, we defined ACE as the accumulated wind energy for each grid cell (i.e., Eulerian approach). The summation of the ACE over the entire domain using the Eulerian approach is exactly equal to the summation of the ACE for all of the TCs using the Lagrangian approach.

The climatological mean of ACE in a grid cell  $A$  can be written as

$$\bar{f}(A) = \iint_C \bar{g}(A_0) \bar{t}(A, A_0) \bar{w}^2(A, A_0) dA_0, \quad (2)$$

where  $f(A)$  is the ACE in a specific grid cell  $A$ ; an overbar indicates the climatological mean;  $g(A_0)$  is the frequency of TC genesis in a remote grid cell  $A_0$ ;  $t(A, A_0)$  is the probability that a TC generated in the grid cell  $A_0$  travels to the grid cell  $A$ ;  $w^2(A, A_0)$  is the mean square of maximum wind speed for TCs located in the grid cell  $A$  but originally generated in grid cell  $A_0$ ; and  $C$  is the entire domain of the North Atlantic over which the integration is performed. Equation (2) indicates that the ACE for each grid cell is influenced by remote (and local) TC genesis, track, and intensity; therefore, the ACE anomaly from the climatological mean results from anomalies in these properties integrated over the entire domain. ACE in a specific period is obtained by considering the anomaly from its climatological mean:

$$\begin{aligned} \bar{f}(A) + f'(A) = & \iint_C [\bar{g}(A_0) + g'(A_0)] [\bar{t}(A, A_0) \\ & + t'(A, A_0)] [\bar{w}^2(A, A_0) + w'^2(A, A_0)] dA_0, \end{aligned} \quad (3)$$

where a prime indicates the anomaly. Subtracting Eq. (2) from Eq. (3) yields the contribution of each term to the total ACE anomaly:

$$\begin{aligned} f'(A) = & \iint_C g'(A_0) \bar{t}(A, A_0) \bar{w}^2(A, A_0) dA_0 \\ & + \iint_C \bar{g}(A_0) t'(A, A_0) \bar{w}^2(A, A_0) dA_0 \\ & + \iint_C \bar{g}(A_0) \bar{t}(A, A_0) w'^2(A, A_0) dA_0 + \text{NL}, \end{aligned} \quad (4)$$

where NL indicates the nonlinear terms defined by

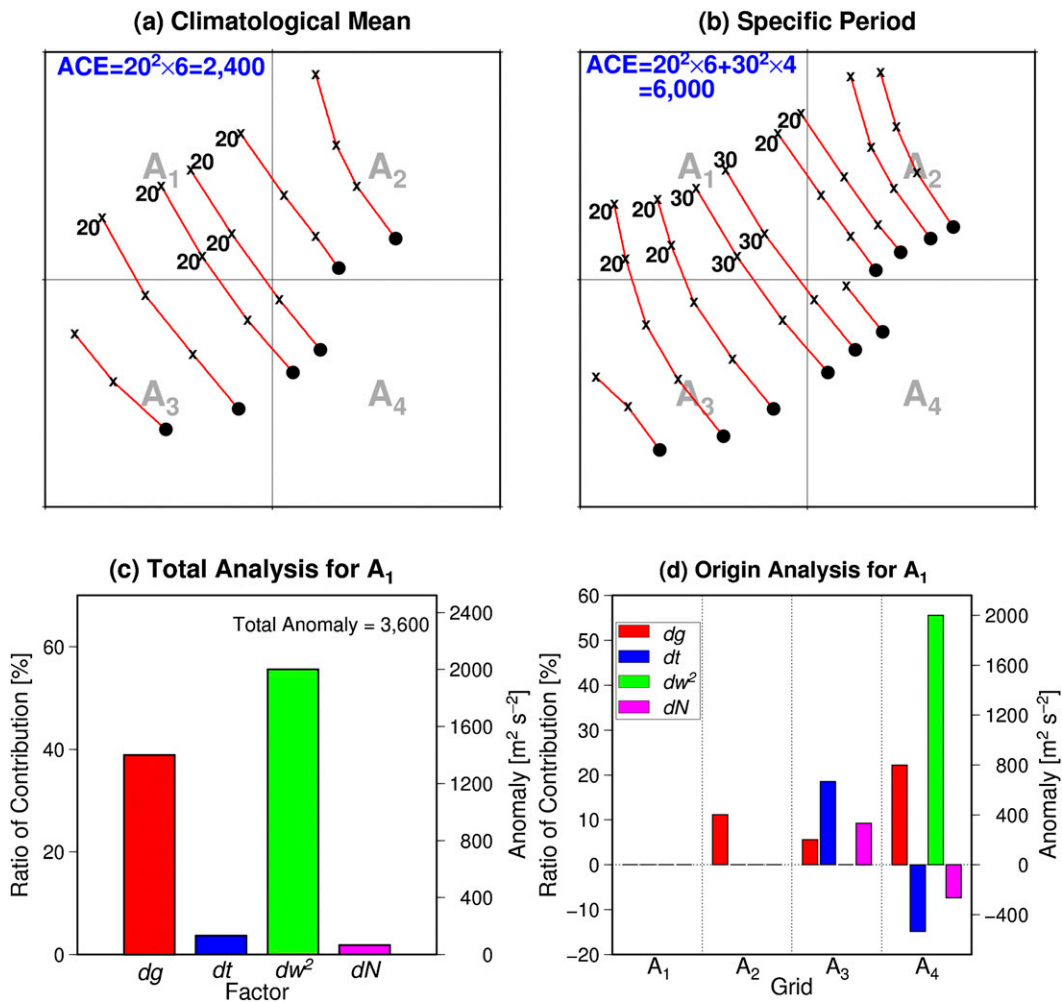


FIG. 2. An example for the empirical statistical analysis for ACE anomaly. Assuming that there are four grids in the entire domain, we focus on the anomaly of ACE in a specific period from the climatological mean in the grid  $A_1$ . (a) Climatological mean TC tracks along with the maximum wind speed ( $\text{m s}^{-1}$ ). (b) As in (a), but for a specific period. (c) Result of the total analysis for identifying the contributing factor for the ACE anomaly in the grid  $A_1$ . (d) As in (c), but using origin analysis for identifying the location of the large impact to the anomaly for the grid  $A_1$ . Black dots (cross marks) in (a) and (b) indicate TC genesis (track) locations. The numbers along with the TC tracks in (a) and (b) indicate maximum wind speed ( $\text{m s}^{-1}$ ). The ACE value ( $\text{m}^2 \text{s}^{-2}$ ) in grid  $A_1$  is shown by the blue text in (a) and (b).

$$\begin{aligned}
 \text{NL} = & \iint_C g'(A_0) t'(A, A_0) \overline{w^2}(A, A_0) dA_0 + \iint_C \bar{g}(A_0) t'(A, A_0) w^2(A, A_0) dA_0 \\
 & + \iint_C g'(A_0) \bar{t}(A, A_0) w^2(A, A_0) dA_0 + \iint_C g'(A_0) t'(A, A_0) w^2(A, A_0) dA_0. \quad (5)
 \end{aligned}$$

Equation (4) is referred to as the total analysis, and reveals the contribution of each of the four factors integrated over the entire domain to the ACE anomaly in a given grid cell. The four factors are (a) TC genesis distribution (first term), (b) TC track (second term), (c) TC intensity (third term), and (d) the nonlinear effect (fourth term). The contribution from the TC genesis term implies that a local ACE anomaly is generated by

varying TC genesis frequency while TC track and TC intensity are kept as climatological mean values over the North Atlantic domain. The TC track effect includes anomalies in TC track direction, TC translation speed, and lifespan.

To facilitate an understanding of empirical statistical analysis, we will look at an example (Fig. 2). Let us suppose there are only four grid cells in the entire domain. As

a climatological mean state (Fig. 2a), on average, two TCs generate in each grid cell of  $A_2$ ,  $A_3$ , and  $A_4$ , and TCs propagate northwestward affecting the frequency of TC occurrence in grid cell  $A_1$  [i.e., climatological mean ACE is  $2400 \text{ (m}^2 \text{ s}^{-2}\text{)}$  in the grid cell  $A_1$ ]. Assume that this occurs in an active TC period (Fig. 2b), which is characterized by an increase in TC genesis frequency for most of the grid cells, an increase in mean maximum wind speed, and changes in TC tracks in a few grid cells. These anomalies in TC properties result in a positive ACE anomaly of  $3600 \text{ (m}^2 \text{ s}^{-2}\text{)}$  in grid cell  $A_1$ . Because the surrounded remote grid cells affect the local ACE anomaly, we should take into account all changes in TC properties (e.g., TC genesis frequency, TC tracks, and TC intensity) over the entire domain to address the relative contribution of each TC property to the ACE anomaly for grid cell  $A_1$ . The total analysis [Eq. (4)] reveals which of the TC properties integrated over the domain contributes to the anomaly in ACE in grid cell  $A_1$  (Fig. 2c). For this example, the increase in mean TC intensity (green bar) is a major contributor to the ACE anomaly in  $A_1$ , followed by the increase in TC genesis frequency (red bar).

The total analysis approach [Eq. (4)] is unable to identify the location of the anomalies that are most important to the local anomaly in ACE. Here, we aim to identify the locations associated with a large contribution to the anomaly in ACE for a specific region. We also conducted an origin analysis to help identify the origin of an anomaly. The effect of a remote grid cell  $A_0$  on an ACE anomaly in a specific region  $B$  (including multiple grid cells) is described by

$$\begin{aligned} f'(B, A_0) = & \iint_B g'(A_0) \bar{t}(A, A_0) \overline{w^2}(A, A_0) dA \\ & + \iint_B \bar{g}(A_0) t'(A, A_0) \overline{w^2}(A, A_0) dA \\ & + \iint_B \bar{g}(A_0) \bar{t}(A, A_0) w^2(A, A_0) dA + \text{NL}. \end{aligned} \quad (6)$$

The first, second, and third terms are the contributions of the anomalies in TC genesis frequency, TC track, and TC intensity, respectively, in the grid cell  $A_0$ , to the ACE anomalies in region  $B$ . Likewise, the fourth term is the nonlinear contribution of the combined effect of TC genesis, track, and intensity anomalies to the ACE changes in region  $B$ . Figure 2d shows the result of origin analysis when the targeted region  $B$  is set as the grid cell  $A_1$  for the example. It is the TC intensity effect in grid cell  $A_4$  that contributes markedly to the ACE anomaly in grid cell  $A_1$ . This is because mean TC intensity increases

from 20 to  $30 \text{ m s}^{-1}$  for the TCs generated in the grid cell  $A_4$  and travel to  $A_1$ . For the remote contributions from grid cell  $A_4$ , the TC genesis factor also contributes positively; however, the contribution is offset by a decrease in the TC track effect because the probability of TC propagation from  $A_4$  to  $A_1$  decreases compared with the climatological mean state. For the remote contribution from grid cell  $A_3$ , the TC genesis and track effects contribute positively to the anomaly in  $A_1$ . The nonlinear effect arises because both TC genesis and TC tracks change simultaneously. For the grid cell  $A_2$ , the TC genesis effect is the only contributor to the positive anomaly in  $A_1$  because other TC properties remain as the climatological mean state.

We had planned to apply empirical analysis to the anomaly for an individual year to analyze linear trends of ACE and PDI and each term contribution. However, the trend analyses require a large number of TCs to reduce sampling errors, especially for the terms  $t(A, A_0)$  and  $w^2(A, A_0)$ . Therefore, it is questionable whether the empirical method can be applied to anomalies in individual years. To increase sample size (Yokoi and Takayabu 2013), we analyzed 41 consecutive and overlapping periods of 7 years each, beginning with 1966–72, then 1967–73, and continuing to 2006–12. By doing so, the interannual fluctuations are smoothed out and we can focus on the linear trend for the data with time scales longer than a decade. The 7-yr running means for the ACE and each term in Eq. (4) generate anomalies from the climatological means and their trends are evaluated and discussed in section 3a. The contribution of each term is evaluated for every grid cell  $A$  ( $10^\circ \times 10^\circ$ ) for the total analysis. The linear trend (or decadal anomaly) for each term in Eq. (6) is computed for the origin analysis and this provides the contribution of each term to the trend (or decadal anomaly) in ACE for region  $B$  as a function of remote grid cell  $A_0$ . When region  $B$  is set as the whole North Atlantic domain, the contribution of each grid cell to the basinwide ACE trend (or decadal anomaly) can be identified for each term.

As mentioned previously, Elsner et al. (2004) pointed out an abrupt shift in TC activity around 1995 (see Fig. 1) so that recent high values of ACE and PDI may be due to decadal variability rather than a linear trend. In section 3d, we also applied empirical analysis to decadal variability to identify contributing factors to the positive anomalies in the most recent decade. In the analysis, the target period is set as 1995–2012, whereas the climatological mean period is set as 1966–2012, and the same empirical analysis, as shown in Fig. 2, is applied.

The overall results for the analysis throughout this study are not sensitive to the running mean period (e.g., 5 or 11 yr), the analysis period (e.g., from 1979 to 2012),

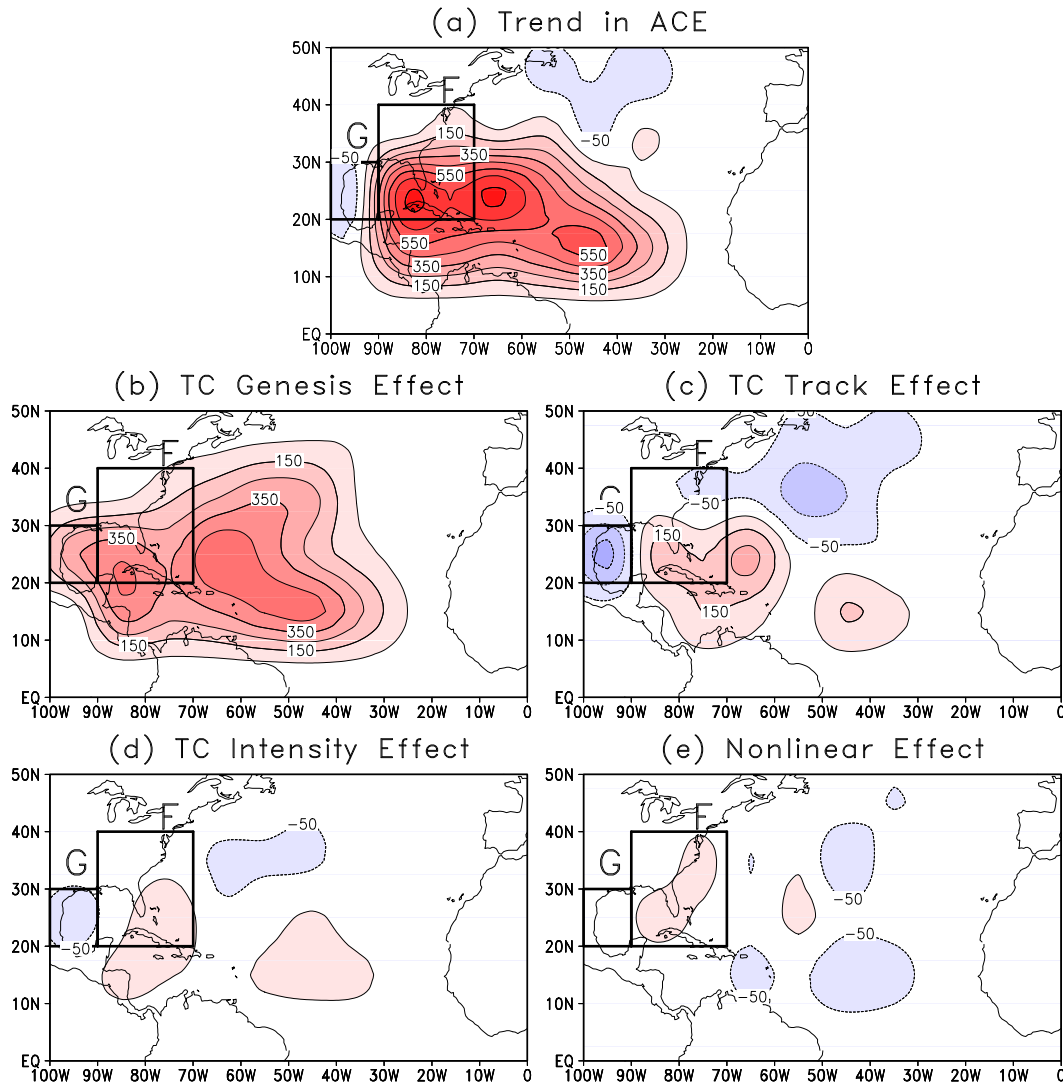


FIG. 3. Linear trend during the period 1966–2012. (a) Trend computed in each  $10^\circ \times 10^\circ$  grid cell for ACE, and the contribution of each term to the trend in ACE by (b) TC genesis effect, (c) TC track effect, (d) TC intensity effect, and (e) the nonlinear effect, as calculated for the total analysis in Eq. (4). Units:  $\text{m}^2 \text{s}^{-2} \text{yr}^{-1}$ . Regions enclosed by rectangles are discussed in the text.

or seasons (e.g., August–October, July–November, and all seasons); however, the nonlinear term becomes larger when the applied grid size becomes smaller (e.g.,  $5^\circ \times 5^\circ$  or  $10^\circ \times 5^\circ$ ) because of the sampling errors described above. However, our overall conclusion remains consistent regardless of grid size.

### 3. Results

#### a. Linear trends

Figure 3 shows linear trends in ACE and also the contribution of each term to the ACE trend derived from the total analysis [Eq. (4)]. The ACE (Fig. 3a)

shows a marked positive trend across almost the entire North Atlantic domain, except for the western quadrant of the Gulf of Mexico and north of the Atlantic. Among the potentially influential factors, TC genesis effects (Fig. 3b) are the primary contributors to the overall ACE trend, indicating that an increase in TC genesis somewhere in the domain caused a positive local trend in ACE. The TC track effect (Fig. 3c) was the second most significant contributor around the Florida Peninsula, showing a southeast–northwest-oriented positive contribution pattern, and two negative contributions in the central–north Atlantic and to the west of the Gulf of Mexico. The latter may be the largest contribution to the negative trend west of the Gulf of Mexico, indicating

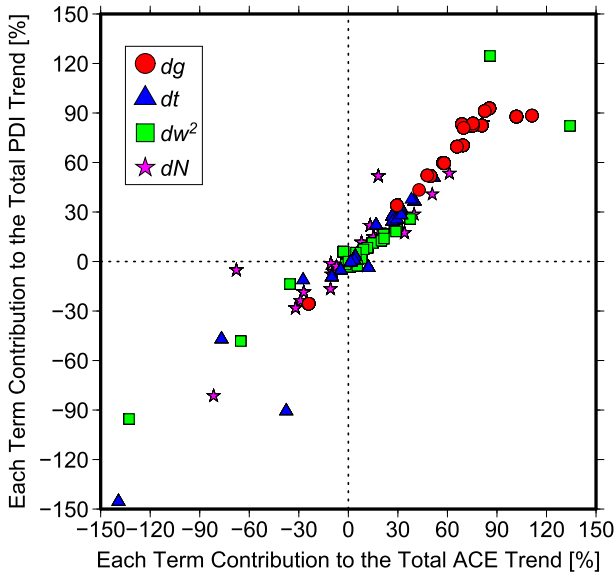


FIG. 4. Scatterplots of all the grid points for each term contribution to the total trend (%) with ACE on the horizontal axis and PDI on the vertical axis. Red circles, blue triangles, green rectangles, and purple stars indicate the TC genesis effect, TC track effect, TC intensity effect, and nonlinear effect, respectively.

that the negative trend in ACE was caused by changes in TC track properties somewhere in the whole domain. The TC intensity effect (Fig. 3d) and nonlinear effect (Fig. 3e) are relatively small compared with other terms, although both effects contribute positive trends near the Florida Peninsula. These results are similar to those

obtained using the PDI (not shown). Figure 4 shows scatterplots of all the grid points for each contribution with ACE on the  $x$  axis and PDI on the  $y$  axis, revealing spatial patterns and relative contributions that are almost same as those obtained from the ACE analysis. The above results indicate that the TC genesis effect is the primary contributor to the overall positive trends in both ACE and PDI.

The total analysis does not identify the locations where the trends have most effect on the local trend in ACE. In contrast, origin analysis [Eq. (6)] can reveal remote contributions to the trend in a specific region. We focus on the coastal regions of F (and G), as shown in Fig. 3, because these coastal regions appear to be crucial to storm related socioeconomic damage and also show marked positive (and negative) trends in ACE and PDI. Figures 5a–c (Figs. 5d–f) reveal remote contributions to the local trend in ACE in region F (G), whereas Figs. 6a–c show the integrated remote contributions over the entire North Atlantic domain to compare the contribution of each term to the local ACE trend.

For region F, a marked positive trend in the TC genesis effect is seen in the so-called main development region (MDR: 10°–20°N, 30°–40°W; Fig. 5a), where the climatological TC genesis frequency is high, indicating that an increase in TC genesis frequency over the MDR is the main contributor to the positive ACE trend around the Florida Peninsula (Fig. 6a). Although weak, the positive trend in the TC intensity effect (Fig. 5c) is also seen around the MDR, indicating that an increase in

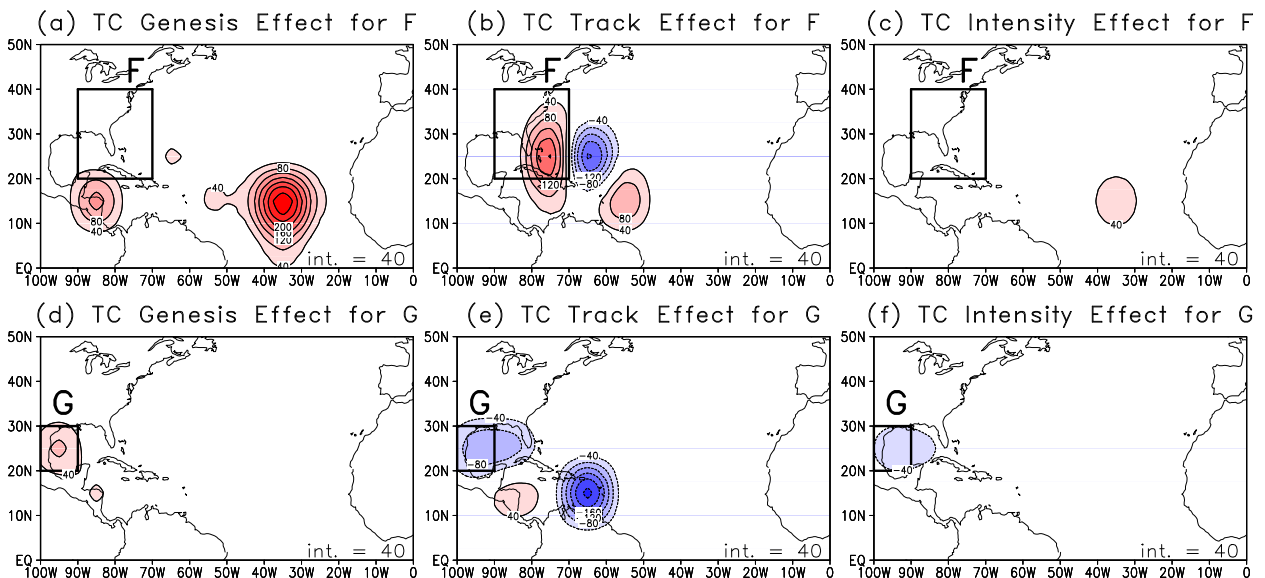


FIG. 5. Remote contribution of each term to trend in a specific region. Factors that influence ACE trend in region F are (a) TC genesis, (b) TC track, and (c) TC intensity, as calculated for the origin analysis in Eq. (6). (d)–(f) As in (a)–(c), but calculated for region G. Contour interval is shown in the bottom-right corner of each panel. Units:  $m^2 s^{-2} yr^{-1}$ .

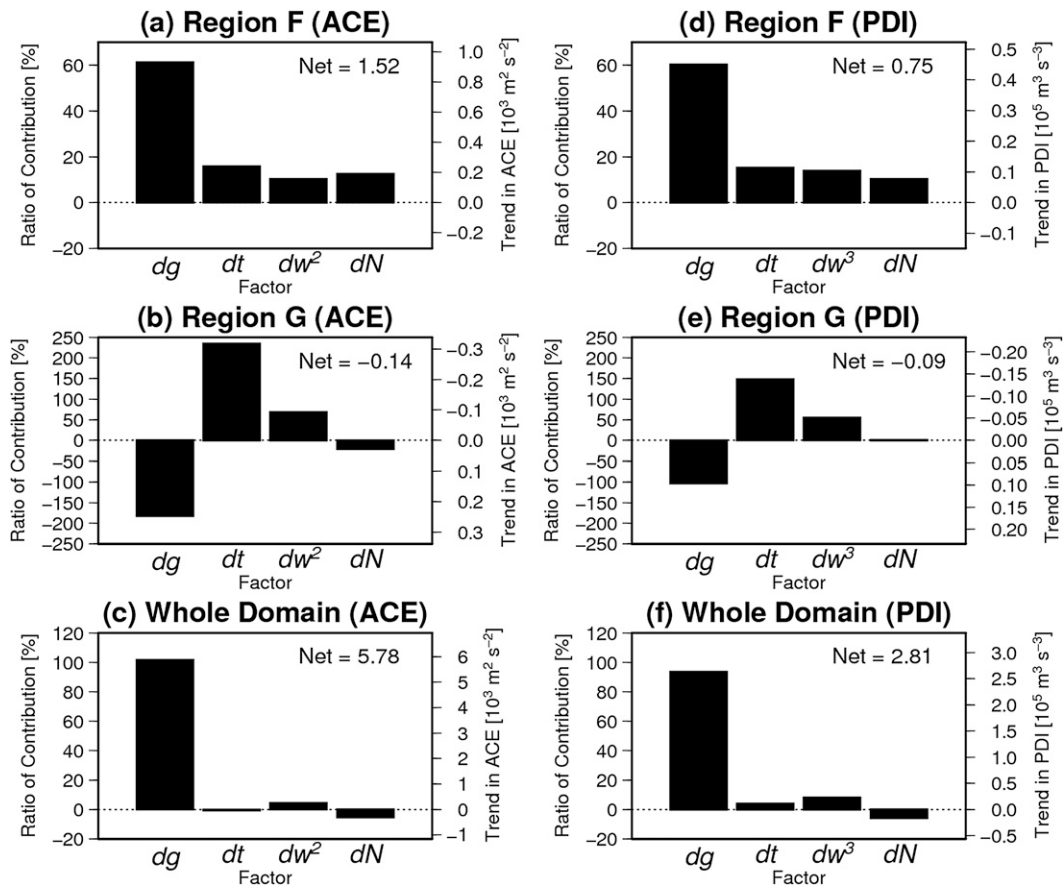


FIG. 6. The contribution of each term to trend in a specific region. Factors that influence ACE trend for a specific region are TC genesis ( $dg$ ), TC track ( $dt$ ), TC intensity ( $dw^2$  or  $dw^3$ ), and the nonlinear effect ( $dN$ ) as calculated for the origin analysis in Eq. (6) and integrated over the whole North Atlantic domain. The targeted regions are (a) region F, (b) region G, and (c) the whole North Atlantic domain, as defined in Fig. 3. The trend for each term is shown on the right axis ( $10^3 \text{ m}^2 \text{ s}^{-2} \text{ yr}^{-1}$ ), whereas the fractional ratio to the net trend is shown on the left axis (%). Net trend is indicated in the upper-right corner of each panel. (d)–(f) As in (a)–(c), but for PDI ( $10^5 \text{ m}^3 \text{ s}^{-3} \text{ yr}^{-1}$ ).

mean TC intensity for the TCs that formed over the MDR and traveled to the region F also contributes to the positive ACE trend around the Florida Peninsula (Fig. 6a). The TC track effect (Fig. 5b) also shows a marked positive trend within region F, indicating that TCs generated over this region are more likely to remain there.

As for the western Gulf of Mexico (region G; Figs. 5d–f and 6b), where ACE shows a negative trend, the TC track effect is a major factor in explaining the negative trend (Figs. 5e and 6b). The two maxima in the negative trend in the TC track effect are located in the Gulf of Mexico and the eastern Caribbean ( $10^\circ$ – $20^\circ\text{N}$ ,  $60^\circ$ – $70^\circ\text{W}$ ), indicating that TCs generated in these regions tend to remain in the region G for shorter periods. The above discussions can be also applied to the results of PDI (Figs. 6d–f), indicating that relative contributions to the regional trends remain regardless of the power of the maximum wind speed.

Although the factors affecting the local trends in ACE and PDI differ from region to region, it is likely that the basin-integrated positive trends in ACE and PDI are mostly driven by the positive trend in TC genesis (Figs. 6c,f).

#### b. Decadal variability

As discussed in section 1 and 2, Elsner et al. (2004) pointed out that an abrupt shift might have occurred in 1995 in terms of the number of major hurricanes (i.e., category 3 or higher on the Saffir–Simpson hurricane destruction potential scale). Because their analysis was based on observed data from 1900 to 2001, it is unclear whether the abrupt change point would still be detected in 1995 if we changed the period to 1966–2012. It would be interesting to see if an abrupt shift is also detected in the number of all TCs as well as the number of major hurricanes. We applied a changing point analysis of reversible jump Markov chain Monte

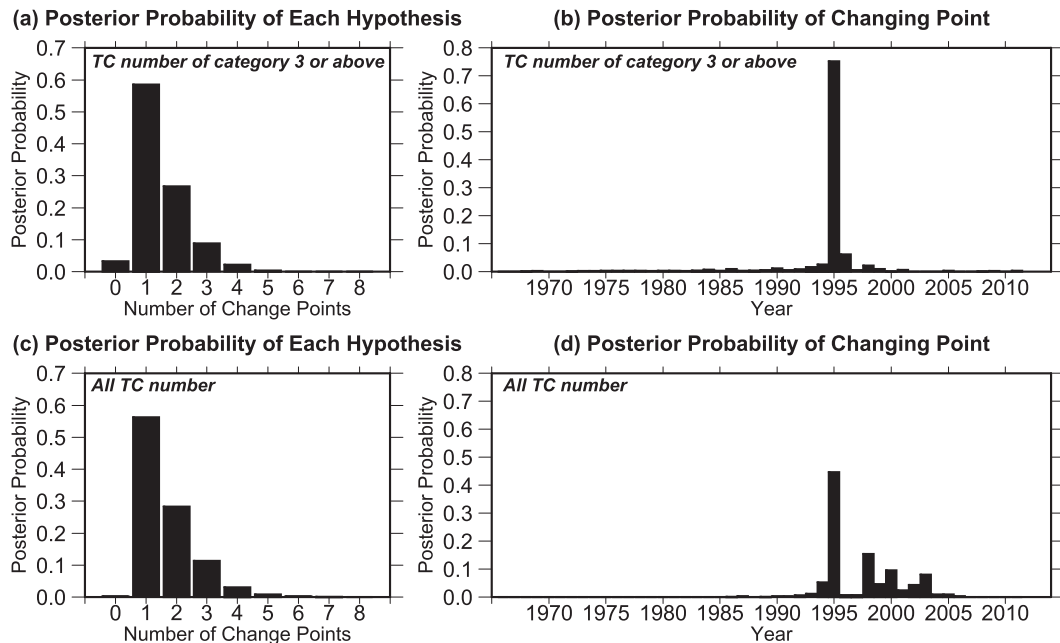


FIG. 7. Results of RJMCMC changing point analysis applied to (a),(b) TC genesis numbers of category 3 or above and (c),(d) all TC numbers. (left) Posterior probability for each candidate hypothesis under which there presumably exists a certain number of abrupt shifts in event series. (right) Posterior probability mass function for the year of the change point under the hypothesis of a single changing point.

Carlo algorithm (RJMCMC) developed by Zhao and Chu (2010) (the program code is available online at [http://www.soest.hawaii.edu/MET/Hsco/Paper/RJMCMC\\_code2.rar](http://www.soest.hawaii.edu/MET/Hsco/Paper/RJMCMC_code2.rar)). The RJMCMC is a Bayesian inference that computes posterior probability for each hypothesis of number of changing points during the analyzed period as well as its associated within-hypothesis parameters such as changing points. Figure 7 shows the results of the RJMCMC when it is applied to the raw data of TC number of category 3 or above and all TC numbers during the period 1966–2012. For both data, the probability of hypothesis of a single change point is the highest (Figs. 7a,c) among any hypotheses of multiple changing points. The probability of the changing point under the hypothesis of a single changing point (Figs. 7b,d) indicates that the most likely choice for the single change point is 1995, a result that is consistent with Elsner et al. (2004).

On the basis of these preliminary results, we decided to apply the empirical analysis to identify contributing factors to the positive decadal anomalies of ACE and PDI during 1995–2012. Figure 8 shows similar results to the trend analysis for ACE (Fig. 3) and the TC genesis effect (Fig. 8b) is the largest contribution to the decadal anomaly. The results of total analysis for the whole North Atlantic domain (Fig. 9) are also mostly consistent with the trend analysis (Figs. 6c,f), although the signs of TC intensity effect and nonlinear effect are

reversed when these values are integrated over the entire domain of the North Atlantic. The results of PDI (Fig. 9a) are almost the same as with ACE (Fig. 9b). Overall, we can conclude that recent positive decadal anomalies in ACE and PDI can be also explained primarily by the positive anomaly in TC genesis frequency.

#### 4. Summary and discussion

To identify the factors responsible for the recent positive trends and decadal anomalies in accumulated cyclone energy (ACE) and power dissipation index (PDI) for tropical cyclones (TCs) in the North Atlantic, a new empirical statistical analysis for the trends and anomalies is applied. The analysis reveals which of four factors (TC genesis, tracks, intensity, and the combined effect of nonlinearity) affects the positive trends and anomalies in ACE and PDI. The analysis indicates that the recent positive increase in TC genesis frequency is the primary contributor to the overall ACE and PDI increase in the North Atlantic. Other factors such as changes in TC tracks (e.g., duration) and TC intensity appear to be minor.

We focus on two coastal regions, which showed marked positive and negative trends in ACE and PDI, to identify the locations where the trends have the greatest

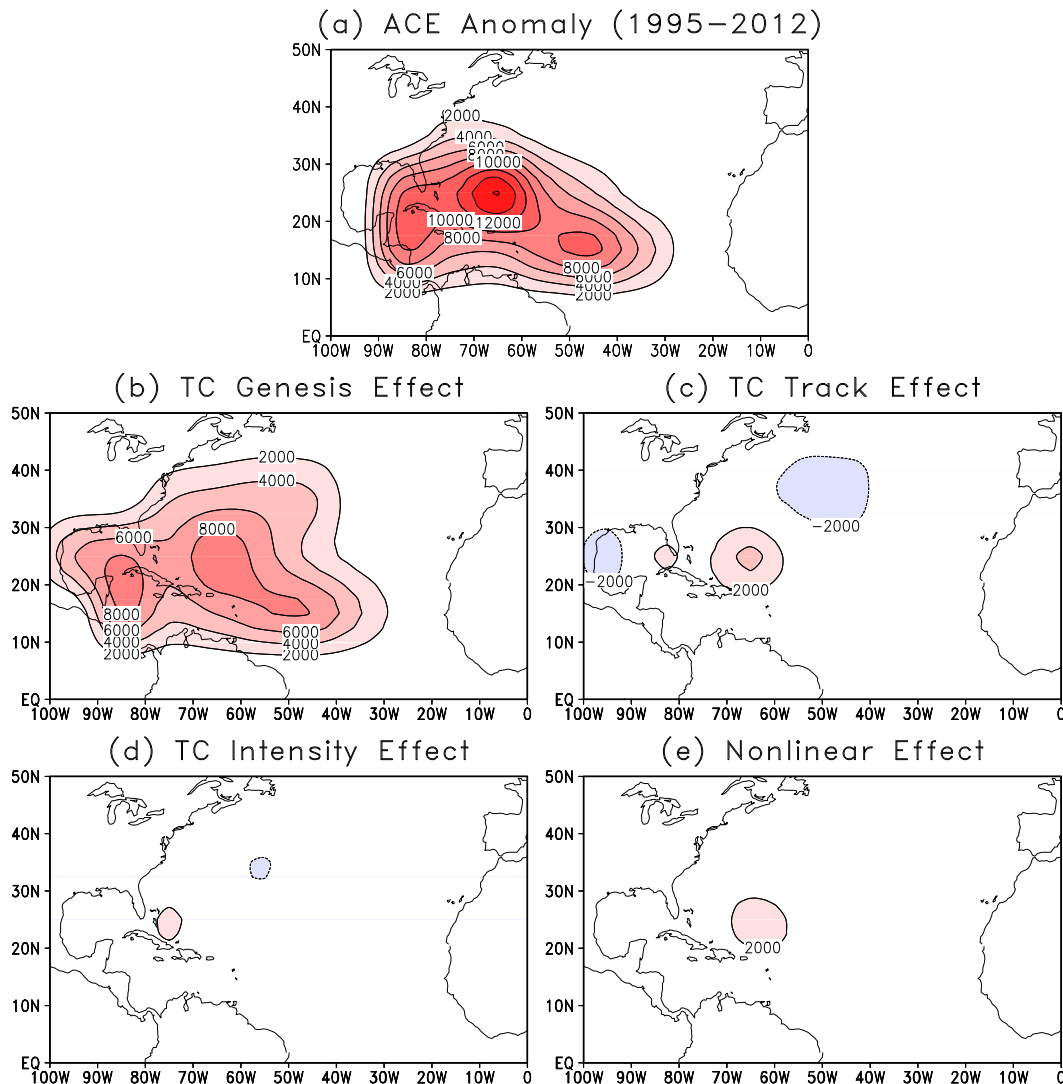


FIG. 8. As in Fig. 3, but for the decadal anomaly of ACE during the period 1995–2012. Units:  $\text{m}^2 \text{s}^{-2} \text{yr}^{-1}$ .

effect on local trends in ACE and PDI. Marked positive trends in ACE and PDI in the Florida Peninsula are primarily attributed to the positive trend in TC genesis frequency in the main development region (MDR). From the results of TC track effect, TCs generated around the Florida Peninsula are more likely to remain there, contributing to positive trends in ACE and PDI around the Florida Peninsula. Although minor, the increase in mean TC intensity for the TCs generated over the MDR also contributes to the positive trends in ACE and PDI around the Florida Peninsula, indicating that the recent positive trend in surface temperature in the MDR region affects not only TC genesis locally (Vecchi and Soden 2007), but also TC intensity remotely. For the western Gulf of Mexico, where ACE and PDI show negative trends, the TC track effect is the major factor

contributing to the negative trends, indicating that TCs that do form in the Gulf of Mexico and the eastern Caribbean Ocean are more unlikely to propagate into the western Gulf of Mexico in recent years. The abovementioned results are also obtained if we apply the empirical analysis to the positive decadal anomalies of ACE and PDI during 1995–2012.

The results in this study indicate that if a (dynamical or statistical) model can predict TC genesis number and its trend correctly, the model has the potential to predict basin-total ACE and PDI, and their trends as well. As evidence of this, recent studies showed that the statistical models, which incorporate the tropical mean SST in the Atlantic and the tropical global mean SST, are skillful at predicting TC number (Vecchi et al. 2010), ACE, and PDI (Villarini and Vecchi 2013).

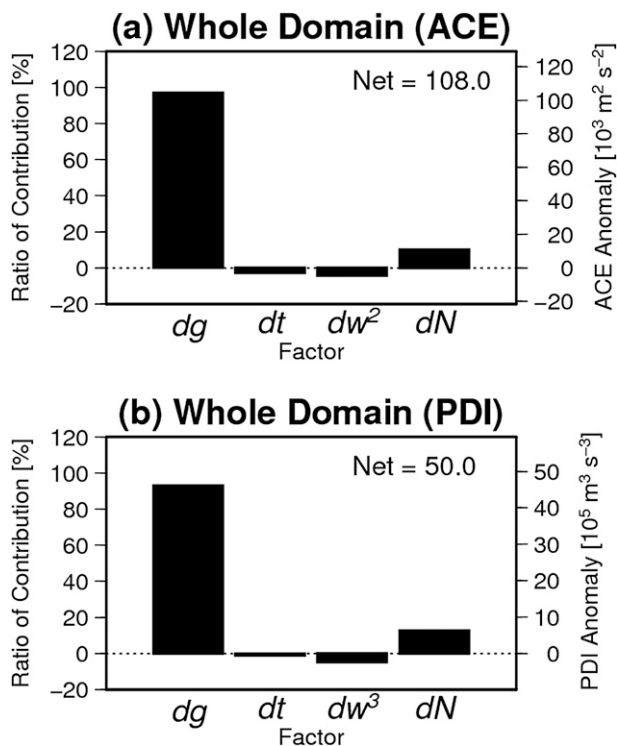


FIG. 9. As in Figs. 6c and 6f, but for the decadal anomaly during the period 1995–2012.

Our study was unable to determine whether the positive trends in ACE and PDI in the North Atlantic are caused by anthropogenic global warming or natural variability. Recent studies have suggested that TC activity (especially TC genesis number) is largely controlled by interannual to multidecadal variability such as ENSO (Chu 2004), the Atlantic meridional mode (Vimont and Kossin 2007), and the Atlantic multidecadal oscillation (Vimont and Kossin 2007). Further studies to apply the current analysis method to future projections using state-of-the-art climate models may help compare the recently observed trend with that induced by global warming.

**Acknowledgments.** This work was conducted under the framework of the “Projection of the Change in Future Weather Extremes Using Super-High-Resolution Atmospheric Models” supported by the KAKUSHIN and SOUSEI programs of the Ministry of Education, Culture, Sports, Science, and Technology (MEXT) of Japan, and sponsored by ONR Grant N000141210450. H.M. was also supported by the “Research on Prediction of Climate and Environmental Change to Contribute to Mitigation Plan Decision against Climate Change” of the Meteorological Research Institute (MRI) of Japan. H.M. thanks Ms. May Izumi for her editorial service.

## REFERENCES

- Bell, G. D., and Coauthors, 2000: The 1999 North Atlantic and eastern North Pacific hurricane seasons [in “Climate Assessment for 1999”]. *Bull. Amer. Meteor. Soc.*, **81** (6), S19–S22, doi:10.1175/1520-0477(2000)81[s1:CAF]2.0.CO;2.
- , S. B. Goldenberg, C. W. Landsea, E. S. Blake, T. B. Kimberlain, J. Schemm, and R. J. Pasch, 2013: Atlantic basin [in “State of the Climate in 2012”]. *Bull. Amer. Meteor. Soc.*, **94** (8), S85–S89, doi:10.1175/2013BAMSStateoftheClimate.1.
- Chu, P.-S., 2004: ENSO and tropical cyclone activity. *Hurricanes and Typhoons: Past, Present and Future*, R. J. Murname and K.-B. Liu, Eds., Columbia University Press, 297–332.
- Elsner, J. B., X. Niu, and T. H. Jagger, 2004: Detecting shifts in hurricane rates using a Markov chain Monte Carlo approach. *J. Climate*, **17**, 2652–2666, doi:10.1175/1520-0442(2004)017<2652:DSIHUR>2.0.CO;2.
- Emanuel, K., 2005: Increasing destructiveness of tropical cyclones over the past 30 years. *Nature*, **436**, 686–688, doi:10.1038/nature03906.
- , 2007: Environmental factors affecting tropical cyclone power dissipation. *J. Climate*, **20**, 5497–5509, doi:10.1175/2007JCLI1571.1.
- Hamed, K. H., and A. R. Rao, 1998: A modified Mann–Kendall trend test for autocorrelated data. *J. Hydrol.*, **204**, 182–196, doi:10.1016/S0022-1694(97)00125-X.
- Klotzbach, P. J., 2006: Trends in global tropical cyclone activity over the past twenty years (1986–2005). *Geophys. Res. Lett.*, **33**, L10805, doi:10.1029/2006GL025881.
- Knutson, T., and Coauthors, 2010: Tropical cyclones and climate change. *Nat. Geosci.*, **3**, 157–163, doi:10.1038/ngeo779.
- Landsea, C. W., 1993: A climatology of intense (or major) Atlantic hurricanes. *Mon. Wea. Rev.*, **121**, 1703–1713, doi:10.1175/1520-0493(1993)121<1703:ACOIMA>2.0.CO;2.
- , 2007: Counting Atlantic tropical cyclones back to 1900. *Eos, Trans. Amer. Geophys. Union*, **88**, 197–202, doi:10.1029/2007EO180001.
- , and Coauthors, 2004: The Atlantic hurricane database reanalysis project: Documentation for the 1851–1910 alterations and additions to the HURDAT database. *Hurricanes and Typhoons: Past, Present and Future*, R. J. Murname and K.-B. Liu, Eds., Columbia University Press, 177–221.
- , B. A. Harper, K. Hoarau, and J. A. Knaff, 2006: Can we detect trends in extreme tropical cyclones? *Science*, **313**, 452–454, doi:10.1126/science.1128448.
- Murakami, H., B. Wang, T. Li, and A. Kitoh, 2013: Projected increase in tropical cyclones near Hawaii. *Nat. Climate Change*, **3**, 749–754, doi:10.1038/nclimate1890.
- , P.-C. Hsu, O. Arakawa, and T. Li, 2014: Influence of model biases on projected future changes in tropical cyclone frequency of occurrence. *J. Climate*, **27**, 2159–2181, doi:10.1175/JCLI-D-13-00436.1.
- Vecchi, G. A., and B. J. Soden, 2007: Effect of remote sea surface temperature change on tropical cyclone potential intensity. *Nature*, **450**, 1066–1071, doi:10.1038/nature06423.
- , M. Zhao, H. Wang, G. Villarini, A. Rosati, A. K. Kumar, I. M. Held, and R. Gudgel, 2011: Statistical–dynamical predictions of seasonal North Atlantic hurricane activity. *Mon. Wea. Rev.*, **139**, 1070–1082, doi:10.1175/2010MWR3499.1.
- Villarini, G., and G. A. Vecchi, 2012: North Atlantic power dissipation index (PDI) and accumulated cyclone energy (ACE): Statistical modelling and sensitivity to sea surface temperature changes. *J. Climate*, **25**, 625–637, doi:10.1175/JCLI-D-11-00146.1.
- , and —, 2013: Multiseason lead forecast of the North Atlantic power dissipation index (PDI) and accumulated cyclone

- energy (ACE). *J. Climate*, **26**, 3631–3643, doi:10.1175/JCLI-D-12-00448.1.
- Vimont, D. J., and J. P. Kossin, 2007: The Atlantic meridional mode and hurricane activity. *Geophys. Res. Lett.*, **34**, L07709, doi:10.1029/2007GL029683.
- Webster, P. J., G. J. Holland, J. A. Curry, and H.-R. Chang, 2005: Changes in tropical cyclone number, duration, and intensity in a warming environment. *Science*, **309**, 1844–1846, doi:10.1126/science.1116448.
- Yokoi, S., and Y. N. Takayabu, 2013: Attribution of decadal variability in tropical cyclone passage frequency over the western North Pacific: A new approach emphasizing the genesis location of cyclones. *J. Climate*, **26**, 973–987, doi:10.1175/JCLI-D-12-00060.1.
- Zhao, X., and P.-S. Chu, 2010: Bayesian changepoint analysis for extreme events (typhoons, heavy rainfall, and heat waves): An RJMCMC approach. *J. Climate*, **23**, 1034–1046, doi:10.1175/2009JCLI2597.1.